Magnetization processes in hybrid magnets

M. Emura, A. C. Neiva, F. P. Missell, K. L. Babcock, J. Ormerod, and S. Constantinides

Citation: Journal of Applied Physics **83**, 7127 (1998); doi: 10.1063/1.367541
View online: http://dx.doi.org/10.1063/1.367541
View Table of Contents: http://scitation.aip.org/content/aip/journal/jap/83/11?ver=pdfcov
Published by the AIP Publishing

Magnetization processes in hybrid magnets

M. Emura, A. C. Neiva, and F. P. Missell[a)]
Instituto de Física, Universidade de São Paulo, C. P. 66318, 05315-970 São Paulo, S.P., Brazil

K. L. Babcock
Digital Instruments, Santa Barbara, California 93103

J. Ormerod and S. Constantinides
The Arnold Engineering Company, Marengo, Illinois 60152

Injection-molded, oriented hybrid magnets consisting of mixtures of $BaO \cdot 6Fe_2O_3$ and MQP-Q (exchange-coupled $Nd_2Fe_{14}B+\alpha$-Fe) are compared to bonded magnets made only from ferrite or MQP-Q. The magnetic fractions of the hybrid magnets consist of 80, 60, or 40 wt % ferrite blended with 20, 40, or 60 wt % MQP-Q. The microstructure was investigated by x-ray diffraction, scanning electron microscopy, atomic force microscopy, and magnetic force microscopy. Atomic and magnetic force microscopy images indicated differences between the physical and magnetic microstructures. Magnetic interactions were studied via isothermal remanence (IRM) and dc-demagnetization (DCD) remanence curves and Henkel plots. In contrast to what is observed in exchange spring magnets, the IRM and DCD susceptibilities of all magnets present peaks of nearly the same width, centered at roughly the same value of the magnetic field, consistent with weak dipolar interactions between magnetic particles. The IRM susceptibilities show structure associated with magnetic inhomogenieties in the samples. © *1998 American Institute of Physics.* [S0021-8979(98)17211-0]

Bonded magnets constitute the fastest growing segment of the permanent magnet market.[1,2] These materials are produced by encapsulating a magnetic powder in a resin or polymer and then compacting or molding the material to the final part shape. The commercially important bonded magnets are based primarily upon ferrite or NdFeB. However, low-neodymium, exchange-coupled alloys are also interesting for bonded magnets because of their good corrosion resistance and low saturation fields. The Magnequench alloy MQP-Q ($Nd_2Fe_{14}B+\alpha$-Fe) has recently been used with barium ferrite to produce hybrid magnets with interesting coercive properties.[2] For a bonded magnet whose magnetic fraction consists of 20 wt % MQP-Q and 80 wt % ferrite, the reversible temperature coefficient of coercivity is approximately zero around and above room temperature. Furthermore, at 100 °C, the coercive field H_c of the hybrid is larger than that of either the bonded ferrite or the bonded MQP-Q. Enhanced hysteresis characteristics due to anisotropic dipole interactions have been observed[3] in composite mixtures $Sm_2Co_{17}/Sm_2Fe_{17}N_3$ and Sm_2Co_{17}/Fe.

In this article, we investigate magnetic interactions in several hybrid magnets and present data on their magnetic and structural properties. The bonded magnets present an ideal opportunity to study systems in which dipole interactions should be the predominant form of interaction between particles.

Five commercial bonded magnet compositions were considered in this work. Three anisotropic hybrid magnets, produced by injection molding, had magnetic fractions consisting of 80, 60, or 40 wt % Ba ferrite blended with 20, 40, or 60 wt % of MQP-Q melt-spun ribbons and a binder of Nylon 12. These have been designated as samples 2401, 2402, and 2403, respectively. An anisotropic magnet consisting only of Ba ferrite is designated as 1060, while an isotropic magnet whose magnetic fraction is MQP-Q is identified as 2203. For the latter two magnets, polyamide was used as a binder. The saturating field requirements as well as the temperature dependence of the coercivity for these magnets have been published previously.[2] For all magnets, we were able to reproduce the catalog density by assuming the volume fraction of the magnetic material to be 60%.

The alignment of these magnets was characterized with a Philips MDP 1880 powder diffractometer using Cu $K\alpha$ radiation. The microstructure was examined with an optical microscope as well as with a Leica Cambridge F440 scanning electron microscope (SEM). Magnetization M measurements between 4.2 and 300 K were made with a vibrating sample magnetometer mounted in a 9 T superconducting coil, while measurements above 300 K were made in a furnace mounted on a 2 T electromagnet. In all cases, M versus H was corrected using an appropriate demagnetization factor.

Images were also obtained using a Digital Instruments D3000 scanning probe microscope. The device allows simultaneous collection of topography data, by Tapping Mode™ atomic force microscopy (AFM), and magnetic stray field data, by LiftMode™ magnetic force microscopy (MFM).[4] The topographical information from each raster line is used to maintain a constant height above the sample surface during collection of the magnetic information to minimize the effect which topological features have on the stray field distribution. In the topological images, light areas are higher than the average and dark areas are lower than the average.

[a)]Electronic mail: fmissell@macbeth.if.usp.br

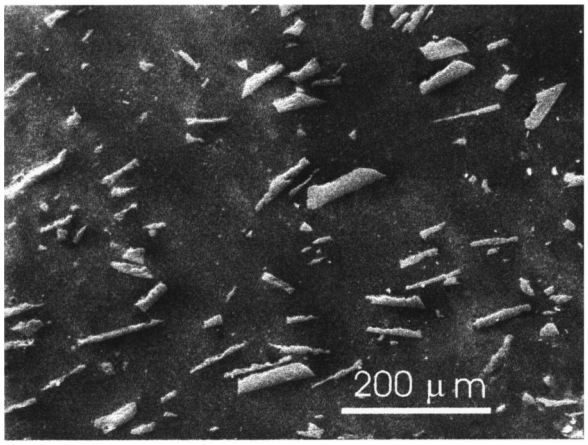

FIG. 1. SEM image of sample 2401 showing inhomogeneous distribution of MQP-Q ribbons.

In the magnetic images, light areas correspond to tip–sample interactions producing a negative force gradient, while positive gradients correspond to dark areas.[4]

In the hybrid magnets, the Ba ferrite grains present a high degree of alignment as can be verified by x-ray diffractograms in which the $(00k)$ peaks of this phase are prominent. Optical metallography and SEM observations show the ribbons of MQP-Q to be randomly dispersed in the ferrite–Nylon 12 matrix. In Fig. 1, a low magnification SEM image of sample 2401 is presented where the random orientation of the MQP-Q ribbons can be seen. A useful way to quantify the degree of alignment of these samples is in terms of the ratio M_r/M_s, where M_r is the measured remanence and M_s is the saturation magnetization, obtained by extrapolating high-field M values to infinite fields using $M=M_s(1-a/H)$. Values of M_r/M_s are presented in Table I. This ratio is seen to decrease as the ferrite fraction of the magnet decreases. Values of $M_r/M_s=0.8-0.9$ are commonly encountered in aligned sintered magnets, while $M_r/M_s=0.5$ is the value expected for noninteracting single-domain particles.

A group of Ba ferrite grains in an unmagnetized sample of 2401 can be clearly seen in Fig. 2(a), which was obtained by AFM. Note the presence of a large ferrite grain in the center of the figure. The magnetic stray fields for the same region of the sample, obtained by MFM, are shown in Fig. 2(b). The magnetic stray fields associated with the large ferrite grain in the center of the figure are very nonuniform over the grain, indicating the presence of two domains in this grain. Furthermore, the stray fields of several small neighboring grains have the same orientation as one of the domains in the large central grain. In general, we can see that the stray field distribution does not coincide with the grain structure of the sample. It is known that magnetic interactions between neighboring grains can lead to collective phenomena, known as interaction domains. The details of intergrain interactions will depend upon exchange, anisotropy, magnetic moment, grain size, and grain misorientation, all of which will affect the stray fields. Interaction domains have been observed in many kinds of magnets, including exchange-coupled nanostructured rare-earth magnets.[5] In the present case, the existence of interaction domains is evidence for locally inhomogeneous magnetization states in the hybrid magnets.

TABLE I. Magnetic characteristics of the bonded magnets.

Sample	M_r/M_s	H_r'(kOe)	H_r(kOe)	Δ_r'(kOe)	Δ_r(kOe)
1060	0.91	3.8	3.9	2.5	2.4
2401	0.75	4.2	4.2	4.0	2.7
2402	0.68	4.9	4.8	4.0	2.9
2403	0.59	4.7	4.3	4.3	3.4
2203	0.54	5.9	5.1	4.1	3.4

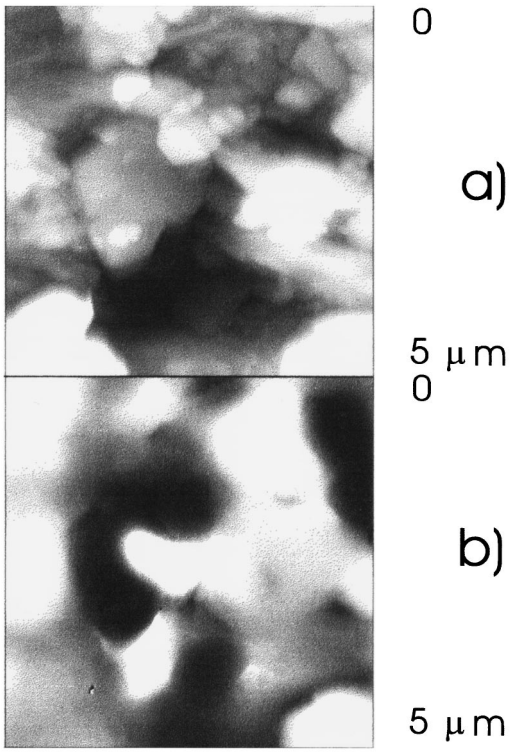

FIG. 2. (a) AFM image of the 5 μm×5 μm region of Ba ferrite in sample 2401. (b) MFM image of the same 5 μm×5 μm region showing stray magnetic fields present in the sample. Note that the magnetic domain structure does not coincide with the grain structure.

A magnetic evaluation of magnetostatic interactions was made using the so-called IRM and DCD remanence curves and Henkel plots. The isothermal remanence (IRM) curve $M_r(H)$ started from an ac-demagnetized state, with the remanent magnetization being measured as a function of increasing positive applied field until positive saturation was obtained. The dc-demagnetization (DCD) curve $M_d(H)$ was measured from a positive saturation condition, with the remanence measured as a function of increasing negative field, until negative saturation was reached. For any system of single-domain noninteracting particles, Wohlfarth showed that $M_d(H)=M_r(\infty)-2M_r(H)$.

In Fig. 3, we show the IRM and DCD susceptibilities, $\chi_r=dM_r/dH$ and $\chi_d=dM_d/dH$, for the five magnets studied. For noninteracting systems, the two curves should be of the same width, should have maxima at the same values of

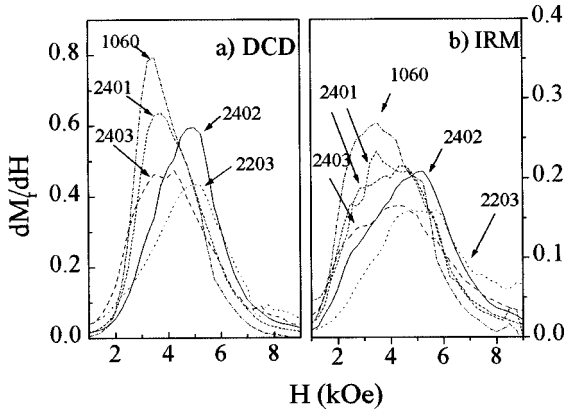

FIG. 3. IRM and DCD susceptibilities of the bonded magnets studied. For magnet 2401, the two IRM curves are for different samples and show different structure.

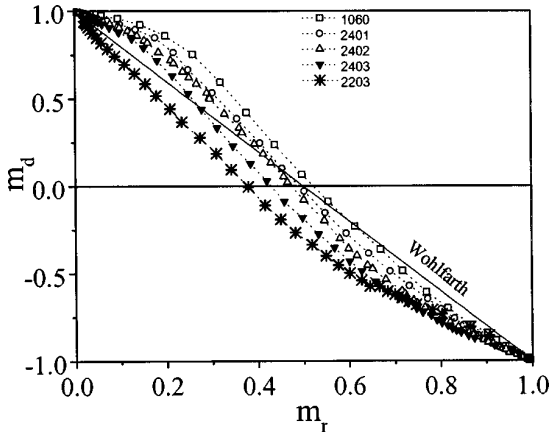

FIG. 4. Henkel plots for all samples, in which the reduced DCD remanence is given as a function of the reduced IRM remanence.

the magnetic field, and the amplitudes should differ by a factor of 2, as can be seen by differentiating the Wohlfarth relation. Values of the widths and centers of the IRM (Δ_r', H_r') and DCD (Δ_r, H_r) curves are given in Table I. It is most remarkable that these predictions are roughly obeyed for the five magnets studied, even though four of them contain varying amounts of exchange-coupled MQP-Q. A recent study[6] of several exchange-coupled NdFeB alloys showed that the amplitude of χ_d was up to 50 times greater than that of χ_r, while the width of the former was about ten times less than the latter. On the other hand, CoNiCr thin films[7] approached the ideal behavior for large values of the Cr underlayer thickness, consistent with a reduction in exchange coupling between grains with increasing Cr underlayer.

In Fig. 3, two χ_r curves are shown for magnet 2401, corresponding to different samples. Each curve presents some structure, not unlike, but smaller than that reported in Ref. 6. However, the structure observed on the two curves corresponding to sample 2401 in Fig. 3 is different from curve to curve. Since our samples clearly present inhomogeneities (see Fig. 1) in the distribution and orientation of the MQP-Q ribbons, we believe this to be the probable cause of the structure observed in χ_r.

Finally, in Fig. 4 we present Henkel plots $[m_d = M_d(H)/M_r(\infty)$ versus $m_r = M_r(H)/M_r(\infty)]$ for the five magnets studied in this paper. The diagonal line corresponds to the Wohlfarth line mentioned above. Points above this line correspond to magnetizing interactions, while points below this line are indicative of demagnetizing interactions. In Fig. 4 there is a clear progression in the behavior of the data as the fraction of MQP-Q is increased (fraction of ferrite is decreased). Sample 1060 shows strong magnetizing interactions at low fields. Data for sample 2401 present an s-shaped behavior, which has been seen frequently in exchange-coupled magnets.[8] This s-shaped curve has been discussed via the Preisach model in terms of a competition between mean-field effects and random interactions.[8] Finally, for sample 2203, whose magnetic fraction is only MQP-Q, all points are in the demagnetizing region of the Henkel plot.

Henkel plots can be discussed in terms of the Preisach model,[9] where one can invoke random interactions and magnetizing or demagnetizing mean-field interactions to explain behavior such as that seen in Fig. 4. Here, we will limit our comments to a comparison with comparable fully dense magnets. For example, the Henkel plot of a fully dense Ba ferrite magnet shows much stronger magnetizing interactions, with nearly all of the data points lying above the Wohlfarth line. For the bonded magnet (1060) shown here, the magnetizing mean-field contributions seem to have been reduced considerably. Similarly, exchange-coupled magnets show an s-shaped Henkel plot, which has been discussed using the Preisach model in terms of a competition between mean-field effects and random interactions.[8] In the present case, sample 2203 appears to have greatly reduced or negative mean-field interactions. Thus, the effect of the binder may be to reduce the mean-field effects in these bonded magnets.

FAPESP, CNPq, CAPES, and FINEP provided financial support. X-ray diffraction and SEM work were performed at the Laboratório de Caracterização Tecnológica-EPUSP.

[1] J. J. Croat, J. Appl. Phys. **81**, 4804 (1997).
[2] J. Ormerod and S. Constantinides, J. Appl. Phys. **81**, 4816 (1997).
[3] J. O'Sullivan, X. L. Rao, and J. M. D. Coey, J. Appl. Phys. **81**, 5124 (1997).
[4] K. Babcock, M. Dugas, S. Manalis, and V. Elings, Mater. Res. Soc. Symp. Proc. **355**, 311 (1995).
[5] W. Rave, D. Eckert, B. Gebel, A. Handstein, R. Schäfer, and K.-H. Müller, *Magnetic Anisotropy and Coercivity in Rare-Earth Transition Metal Alloys* (World Scientific, Singapore, 1996), pp. 297–306.
[6] L. H. Lewis, D. O. Welch, and V. Panchanathan, J. Appl. Phys. **81**, 4422 (1997).
[7] P. I. Mayo, K. O'Grady, P. E. Kelly, J. Cambridge, I. L. Sanders, T. Yogi, and R. W. Chantrell, J. Appl. Phys. **69**, 4733 (1991).
[8] See, for example, D. R. Cornejo, M. Lo Bue, V. Basso, G. Bertotti, and F. P. Missell, J. Appl. Phys. **81**, 5588 (1997), and references therein.
[9] V. Basso and G. Bertotti, IEEE Trans. Magn. **30**, 64 (1994).